JOURNAL OF MATERIALS RESEARCH AND TECHNOLOGY 2021;10:349–362

Available online at www.sciencedirect.com

jmr&t Journal of Materials Research and Technology

journal homepage: www.elsevier.com/locate/jmrt

Original Article

Dynamic response of aluminium sheet 2024-T3 subjected to close-range shock wave: experimental and numerical studies

Amin Bassiri Nia [a], *Ali Farokhi Nejad* [a,b], *Li Xin* [c], *Amran Ayob* [a], *Mohd Yazid Yahya* [a,**], *Seyed Saeid Rahimian Koloor* [d,e,*], *Michal Petrů* [d], *Shukur Abu Hassan* [a]

[a] *Center for Advanced Composite Materials, School of Mechanical Engineering, University Technology Malaysia, Malaysia*

[b] *Department of Mechanical and Aerospace Engineering, Politecnico di Torino, Torino, Italy*

[c] *National Laboratory of Solid State Microstructures & Department of Material Science and Engineering, Nanjing University, Jiangsu, China*

[d] *Institute for Nanomaterials, Advanced Technologies and Innovation (CXI), Technical University of Liberec (TUL), Studentska 2, Liberec, 46117, Czech Republic*

[e] *Department of Aerospace Engineering, Faculty of Engineering, Universiti Putra Malaysia, Serdang, 43400, Malaysia*

ARTICLE INFO

Article history:
Received 16 October 2020
Accepted 7 December 2020
Available online 13 December 2020

Keywords:
Near-field shock wave
Stand-off distance
Dynamic behaviour
Finite element method aluminium alloy sheet
Failure mechanics

ABSTRACT

This present study investigates experimentally and numerically the behaviour of 1 mm thick aluminium 2024-T3 alloy sheets from near field shock waves. A comparison and examination are undertaken with respect to global deformation and plastic damage formation from two different stand-off distances of 4 mm and 50 mm that were exposed to a constant charged mass. A 4-cable instrumented pendulum blast set-up was used to carry out and monitor the blast test. The results of the blast test were subsequently used to simulate the pressure history for different stand-off distances. The simulation involved implementing a user subroutine in ABAQUS/Explicit solver to model non-uniform pressure fields for use in finite element simulation. The results provided a strong alignment of the numerical method when compared with the experimental data. The main outcome of this study is to show the significant effect of the changing damage from highly localised perforation to global deformation when the stand-off distance is changed from 4 mm to 50 mm.

* Corresponding author.
** Corresponding author.
E-mail addresses: yazidyahya@utm.my (M.Y. Yahya), s.s.r.koloor@gmail.com (S.S. Rahimian Koloor).

https://doi.org/10.1016/j.jmrt.2020.12.029

1. Introduction

Aluminium alloys are widely used in automotive, aviation, and naval industries as a result of their high specific strength, effective energy absorption, excellent corrosion resistance, and good formability. These alloys can bear dynamic shock loading—as in cases of road and air crashes. Moreover, aluminium sheets are commonly used in functionally graded material as a face-sheet, where its cladding ability, good formability, and adhesive bonding all provide manufacturers incentives to use aluminium sheets in their products.

Many structures have been proposed to protect against blast loading such as polymeric composite panels, fibre metal laminates (FML), functionally graded material, etc. However, the most dominant responses from structures, in terms of energy absorption and permanent deflection, can be narrowed down to the metallic panels in protective walls [1,2]. In conducting experimental or numerical investigations, many variables may contribute to different effects. Hence, to examine the effect of test variables several tests are required. Impact testing on metal alone is a challenging task due to the various failure modes that are observed, depending on its ductility [3,4]. Some impulsive experiment tests were conducted to investigate the response on steel sheets [5] and the observations were large inelastic deformation (mode I), tensile tearing (mode II) and transverse shear rapture (mode III). These failure modes were defined for beams, circular and square plates [6–8]. A reliable theoretical or numerical analysis on the dynamic response of structures made of different materials is still a formidable task.

To understand the damage processes that are caused by localised high rate explosive wave on metallic structures, numerical simulation is an interesting approach [9,10]. Numerical models have been used to predict structure behaviour against impulsive loading across numerous investigations. In the earliest models to simulate localised blasts, a constant pressure load was applied to an area equivalent to the charged or burn diameter. In this method, the constant pressure was applied in a few milliseconds which was usually taken as the time for the explosion wave to pass the charge length. This method proved successful when the geometry was large and stand-off distance (SOD) to the sample plates was sufficiently far enough [11]. A variation of this method was presented by Bimha [12] who modelled the impulsive load acting as a constant pressure over the charge area with the decay function to the edge of the plate. Based on a comparison with the experimental plate deflection profiles, the decay constant was found for variations in charge radius as a function of plate radius/width. In an extended method by Balden and Nurick [13] the AUTODYN commercial software was used to obtain the pressure profile for a localised blast load. The pressure profile was based on the profile of the maximum pressure that was obtained from the simulations. The pressure magnitude for the profile was adjusted so that the applied impulse corresponded with the measured experimental ballistic pendulum impulse [14]. This method is one of the most reliable methods to simulate the impulsive pressure profile [6–8,15]. Despite valuable efforts to generate consistent theoretical or mathematical models in overcoming obstacles,

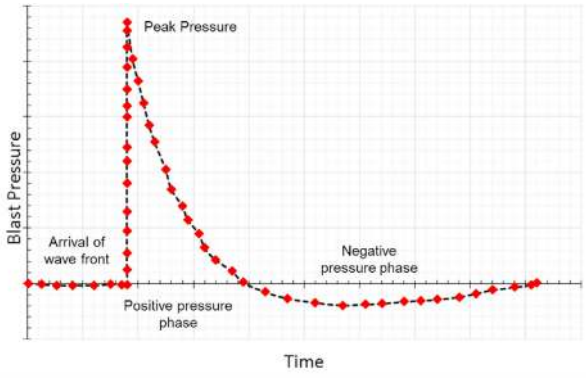

Fig. 1 – The general form of pressure-time history after the explosion [18].

the validity of such models and employing these models as a predictive tool for metallic sheets under impulsive loading is still limited. This present research investigates the effect of different parameters in a blast test on aluminium sheet 2024-T3. Two values of SOD were considered as close-range impulsive loading on square aluminium panels with all four edges fully clamped. The main objective of this study is to demonstrate that the change of SOD from 4 mm to 50 mm causes a significant effect on the damage variation, from a highly localised perforation to a global deformation. However, regarding the case with a constant impulse, the pressure reduction factor on exposed areas and the pressure-time reduction factor plays a crucial role and shows a more destructive effect on the target that is subjected to a SOD of 50 mm. The tests employed a four-cable ballistic pendulum with corresponding laser displacement to record the impulse. The experiment provided material, geometrical, loading, and boundary conditions data for the subsequent phase of the finite element (FE) model in numerical simulation. The model was used to simulate different loading conditions and highlights dynamic responses and blast pressure distributions parameters in close-range explosion.

2. Experimental procedure

2.1. *Blast overview*

When a solid explosive material is charged, it is converted to a hot and high-pressure gas with a transient maximum temperature of about 3000 °C and a peak pressure of up to 40 GPa [16,17]. The high velocity (6000–8000 m/s) compressed air produces a shock wave with discontinuities in pressure, density, temperature, and velocity [8,17]. The instantaneously expanded gas contains extreme levels of compressed air particles which apply pressure on all the surfaces they encounter. In generating the high pressure, the gas from the charged mass expands rapidly to about 4000 times the original volume of the explosive material [18]. The shock front is a characteristic of a blast wave that changes all the gas dynamic conditions, including static pressure, velocity temperature, density, and flows [19,20]. The maximum amplitude of the shock front pressure can be observed immediately after

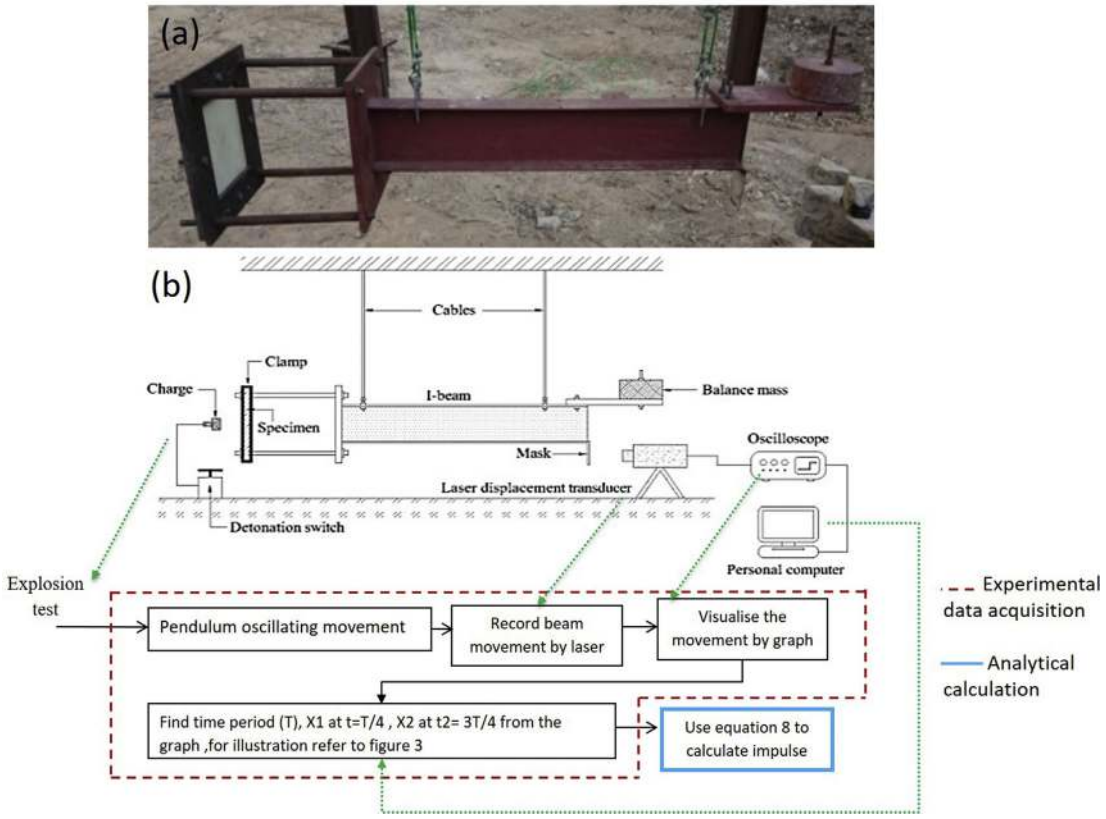

Fig. 2 – The blast test set up (a) four-cable pendulum blast system. (b) Schematic of the four-cable pendulum.

reaching the encountered surface. Subsequently, it decays exponentially with time and is followed by a negative phase. The shock waves can produce a high impulsive amplitude over a very short time, typically within 0.01–1 s, depending on the mass and SOD of explosive material [18]. The air shock wave, in turn, applies a high strain rate (typically between ~100 and 10,000 s^{-1}) loading on the structure which can cause severe dynamic deformation, vibrations, and damage [21,22]. The peak point of air shock wave followed by a sharp decay, is represented in Fig. 1.

The positive region of the overpressure curve decays exponentially over time, and can be calculated by the modified Friedlander expression [17,23]:

$$P = P_{max}\left(1 - \frac{t}{t_d}\right)e^{-\alpha t/t_d} \tag{1}$$

where P is the impulse pressure at time t, P_{max} is the peak pulse when t is zero (i.e. arrival time of the wave front), and t_d is the time period after the wave front.

Generally, explosive tests are categorised into three groups based on stand-off distance i.e. near-field, mid-range field, and far-field explosive tests. Many studies have been carried out for mid-range [17] and far-field explosive tests [24]. The previous research investigated complex dynamic structural responses for far-field air blast and different materials. However, less attention has been paid to the near-field tests. When an explosion occurs in a near-field condition, the shock wave propagates from the source to the structure front face and is reflected after the collision. When the shock wave has enough time to reach the structure in far-field or weak explosions, the peak pressure is calculated in terms that are dependent on the weight (W) and SOD of the explosive charge (TNT equivalent), by:

$$P_{max} \cong 53.9\left(\frac{W^{0.33}}{D}\right)^{1.13} \tag{2}$$

Dependent on the SOD position, the air pressure that results from the shock wave decays over time and with increasing distance from the blast source. Some parts of air pressure are reflected when the shock wave collides with the surface of the specimen and other rigid walls such as the explosion chamber. This phenomenon generates a negative pressure below the ambient pressure after the initial positive pressure phase. The negative phase tends to be longer in duration than the positive phase yet at a much lower amplitude. Therefore, it needs the additional air particles contained in the shock wave to be brought to rest and further compressed, resulting in a higher reflected overpressure on rigid surfaces than the incident overpressure [25]. Generally, positive blast loads are far more damaging to materials and structures than negative phase loads [26]. The loading of a shock wave is estimated in terms of the impulse (I) or energy flux density (E), which are respectively defined as [8]:

$$I = \int_0^t p(t)dt \tag{3}$$

and

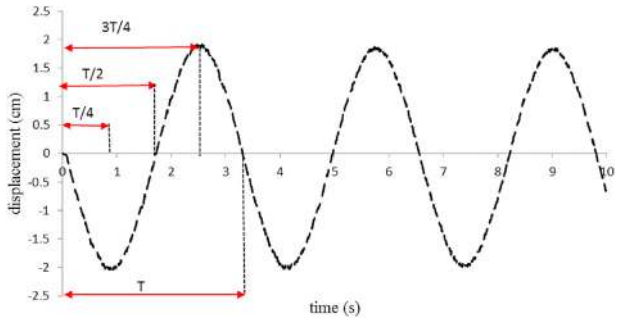

Fig. 3 – Pendulum motion data recorded by laser for 10 *g* spherical emulsion explosive at 4 mm stand-off distance.

$$E = \frac{1}{\rho_0 c_0}\left(1 - A\,P_{max} - B\,P_{max}^2\right)\int_0^t P^2(t)dt \tag{4}$$

where A and B are constant parameters for post-flow velocity correlation. ρ_o and c_o are the initial density and speed of sound is propagating in the air.

2.2. Experimental data acquisition

The blast load was generated by detonating the emulsion explosive which is spherical in shape, resulting in an impulse velocity of 5200 m/s. The four-cable pendulum blast system (Fig. 2a) was used to measure the blast intensity. The aluminium sheets were clamped in front of the ballistic pendulum, exposing an area of 260 mm × 260 mm facing the charge. The explosive was located in line with the centre of aluminium sheet at 4 mm and 50 mm stand-off distances. This setup is designed to provide different blast pressure distribution on the exposed area of the sheet panels (Fig. 2b). The impulse is calculated from the oscillating movement of the pendulum from the explosion. The movement of the pendulum was recorded using laser Micro-Epsilon LD1607-200. Fig. 2b represents the block diagram of input variables from experiment to analytical solution.

Furthermore, the motion formula for a four-cable pendulum blast system [26,27], is used to calculate the impulse from detonation. The general solution for beam movement is shown by Eq. (5).

$$X = e^{-\beta t}\,x_0 / \omega \sin(\omega t) \tag{5}$$

where X is global displacement, β is the time constant, and $\dot{x}_0$ is local initial speed. Two specific solutions, for time $t_1 = T/4$ and $t_2 = 3T/4$, are used as shown by Eqs. (6) and (7) respectively.

$$X_1 = e^{\frac{-\beta T}{4}}\dot{x}_0 T/2\pi \tag{6}$$

$$X_2 = e^{\frac{-3\beta T}{4}}\dot{x}_0 T/2\pi \tag{7}$$

and finally, the impulse (*I*) can be calculated by the following expression,

$$\beta = \frac{2\ln\frac{x_1}{x_2}}{T},\quad I = M_T\,\dot{x}_0 = M_T\,\frac{x_1 2\pi}{T}\,e^{\beta T/4} \tag{8}$$

The impulse intensity for time period (*T*), the total mass (M_T) and β are specified for the present setup. $\beta = 0.0268$, $M_T = 165$ kg, and $T = 3.24$. Fig. 3 shows the recorded oscillating motion data from the pendulum mechanism from the spherical emulsion detonation (10 *g*) at 4 mm SOD on the aluminium 2024-T3 sheet. Here, $x_1 = 20.1848$ mm and $x_2 = 19.3266$ mm. Therefore, from Eq. (8) the impulse is 6.6 N.s.

2.3. Aluminium 2024-T3 under the blast loading

In the present study, aluminium sheets with a 1 mm thickness were subjected to 10 g mass of explosive at different stand-off distances. Fig. 4 shows the blast test setup of the clamped Al2024-T3 sample with a 4 mm SOD.

The material properties of AL 2024-T3 from previous research is taken into account [28,29]. For simulation, considering the high strain rate loading, the empirical Johnson–Cook model was used in the stress equation, as expressed in Eq. (9).

$$\bar{\sigma} = \left[A + B\left(\bar{\varepsilon}^{pl}\right)^n\right]\left[1 + C\ln\left(\frac{\dot{\varepsilon}^{pl}}{\dot{\varepsilon}_0}\right)\right]\left(1 - (T^*)^m\right) \tag{9}$$

where $\bar{\sigma}$ is the rate-dependent yield stress, $\bar{\varepsilon}^{pl}$ is the equivalent plastic strain, *A*, *B* and *n* are material parameters, *C* and $\dot{\varepsilon}_0$ are the strain-rate constant and the reference strain rate, respectively. These material constants are extracted below, at transient temperature (*T**). In Eq. (10), $\bar{\varepsilon}_D^{pl}$ is the equivalent plastic strain at damage initiation, and d_1 to d_4 are failure parameters. The Johnson–Cook model parameters for the AL 2024-T3 alloy are summarised in Table 1.

$$\bar{\varepsilon}_D^{pl} = \left[d_1 + d_2\exp\left(\frac{d_3 P}{q}\right)\right]\left[1 + d_4\ln\left(\frac{\dot{\bar{\varepsilon}}_{pl}}{\dot{\varepsilon}_0}\right)\right] \tag{10}$$

3. Numerical model

3.1. Shock wave modelling

A significant structural deformation occurs during an infinitesimal time-period and it undergoes two response phases. The first phase is the compression through-thickness and the

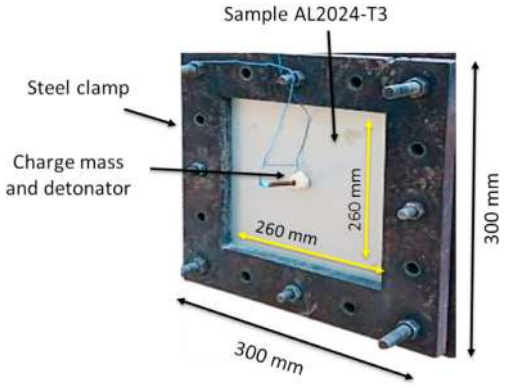

Fig. 4 – Aluminium sheet 2024-T3 clamped in the fixture for the blast test.

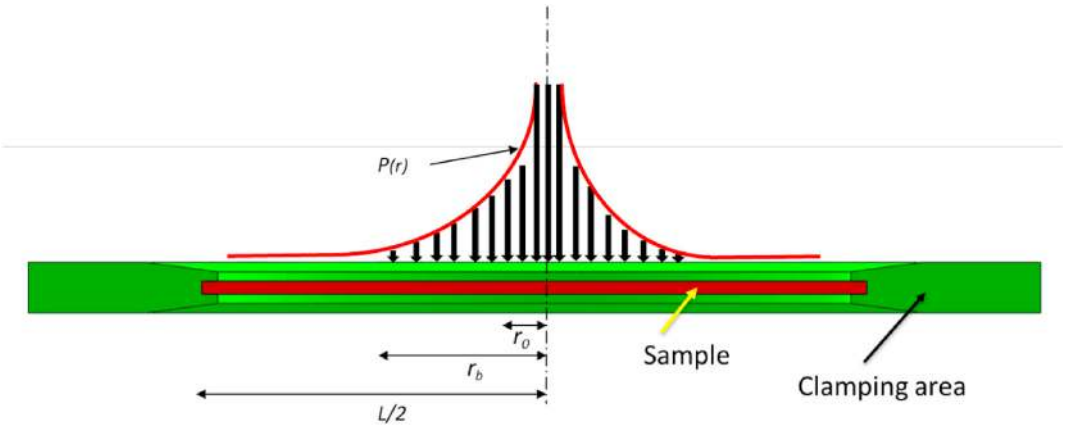

Fig. 5 – The pressure distribution pattern over different positions of the Al 2024-T3 sheet sample.

second is the overall time response. Therefore, tracing the pressure pulse over time should be considered as an important factor to model shock waves. The pressure history is highly dependent on the SOD position and mass of charge. In this study, in order to model the localised impulsive (blast) loading an explicit form of AUTODYN was used to find the pressure distribution as a function of position and time [14]. The pressure can be a function of location which means for different positions of the exposed areas the pressure differs. The pressure distribution pattern over different positions of the sample is shown schematically in Fig. 5. Moreover, the pressure is a function of time which means for close-field explosions the first part of the pressure time-factor increases and in the second part the pressure time-acting factor decreases by an exponential function.

Hence, the basic input to the numerical simulation is to find the pressure distribution as a function of time and location, from the explosion of the charged mass. The blast test is modelled in AUTODYN using the 2D explicit nonlinear model by couple method (modelling air and explosive separately). The air is modelled as an ideal gas. The material properties for air and aluminium 2024-T3 are listed in Table 1. A 14.6 mm radius spherical shape of the explosive is modelled, and the EOS-JWL parameters for explosive are selected from [29]. The individual gauges are defined in the software to provide the pressure-time history and pressure-position history. Fig. 6a illustrates the model of spherical emulsion (10 *g*) in 4 mm stand-off distance and Fig. 6b shows the pressure contour after 150 μs.

From the pressure acting-time history for individual gauges the approximation pressure pattern from AUTODYN can be found [11]. When the mass is charged in very close range, the impulse pressure does not have enough time to convert to a uniform distribution over the sheet blank. Therefore, applying different individual gauges in different locations to find the pressure-time history is essential. Gauges 1 to 5 are 4 mm apart, and Fig. 7a shows that the pressure distribution between the gauges is almost uniform. Gauges 6 to 12 cover 84 mm, from 6 mm to 90 mm (Fig. 7b). The approximate pressure distribution at a radial distance from the centre of the plate and related acting time factor are shown in Fig. 8a and b [30].

Figs. 7 and 8 both show that by increasing the time and distance from the centre of panel, the pressure degrades exponentially by a function which has been used by different researchers [10,31]. For higher SOD the first part of pressure acting time is negligible. Fig. 9 shows the results of the pressure history for 50 mm SOD and 10 *g* explosive. The maximum peak reflected pressure of 60 MPa was reached and the time reduction factor was obtained from AUTODYN solution. The time duration was 55 μs (from 20 μs to 75 μs). Figs. 7–9 show the approximation functions of applied pressure histories for SODs 4 mm and 50 mm. The maximum standard error for all cases was less than ±4% which are indicated with error bars.

Furthermore, Eqs. (11) and (12) present the pressure-history function and time-history function for 10 g emulsion explosive at 4 mm SOD. In the following equations, the two parameters x_k and z_0 have a significant role in influencing the pressure distribution. The pressure decay factor on position (x_k) which influences the pressure degradation on the exposed area is sensitive to stand-off distance SOD. The pressure decay factor with time (z_0) is used to control the effect of time on the pressure after the explosion [10].

$$P(r) = \begin{cases} P_0 \quad if\ r \le r_0 \\ P_0 e^{-xk(r-r0)} \quad if\ r_0 < r \le r_b \\ 0 \quad if\ r > r_b \end{cases} \tag{11}$$

where, $r_0 = 4$ mm, $x_k = 0.0675\ \frac{1}{mm}$, $r_b = 90$ mm are found from approximation function.

Table 1 – AL 2024-T3 Johnson Cook parameters.

	Elastic properties			Johnson–Cook parameters					Damage parameters			
parameters	ρ	E	ϑ	A	B	C	n	m	d_1	d_2	d_3	d_4
unit	(kg/m^3)	(GPa)	–	(MPa)	(MPa)	–	–	–	–	–	–	–
value	2690	74	0.29	369	684	0.0083	0.73	1.7	0.13	0.13	−1.5	0.011

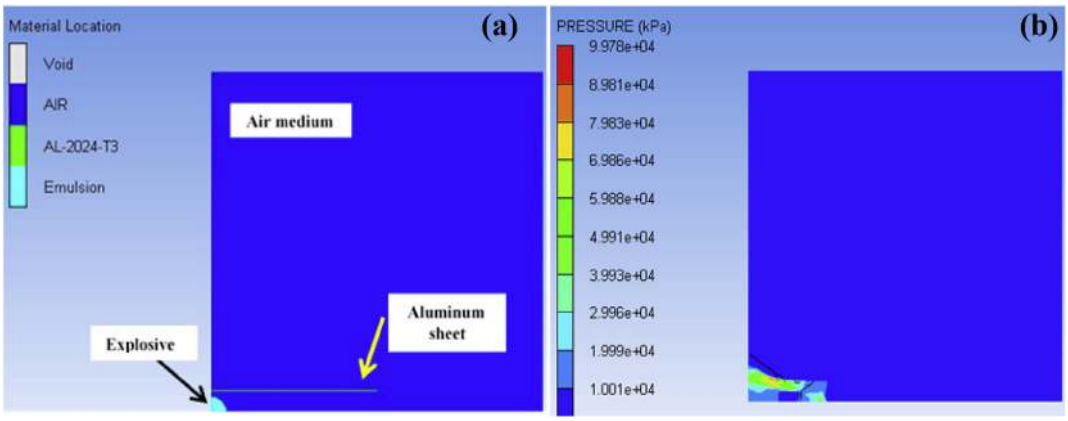

Fig. 6 – (a) AUTODYN 2D model for 10 g emulsion and (b) pressure distribution for after 150 μs.

$$P(t)=\begin{cases} 0 & \text{if } time \le t_{\,death} \\ time/t_{reach} & \text{if } t_{\,reach} < time \le t_{\,peak} \\ e^{-z0\left(time-t_{\,peak}\right)/t_{\,death}} & \text{if } t_{\,peak} < time \le t_{\,death} \\ 0 & \text{if } t > t_{\,death} \end{cases} \quad (12)$$

where arrival time (t_{reach}) = 3 μs, the time at peak reflected pressure ($t_{\,peak}$) = 5.5 μs, and $t_{\,death}$ = 25 μs, z_0 = 7.8 (unitless) are extracted from the AUTODYN output.

For 50 mm SOD, the general form of pressure distribution function on exposed areas is similar to 4 mm SOD with the

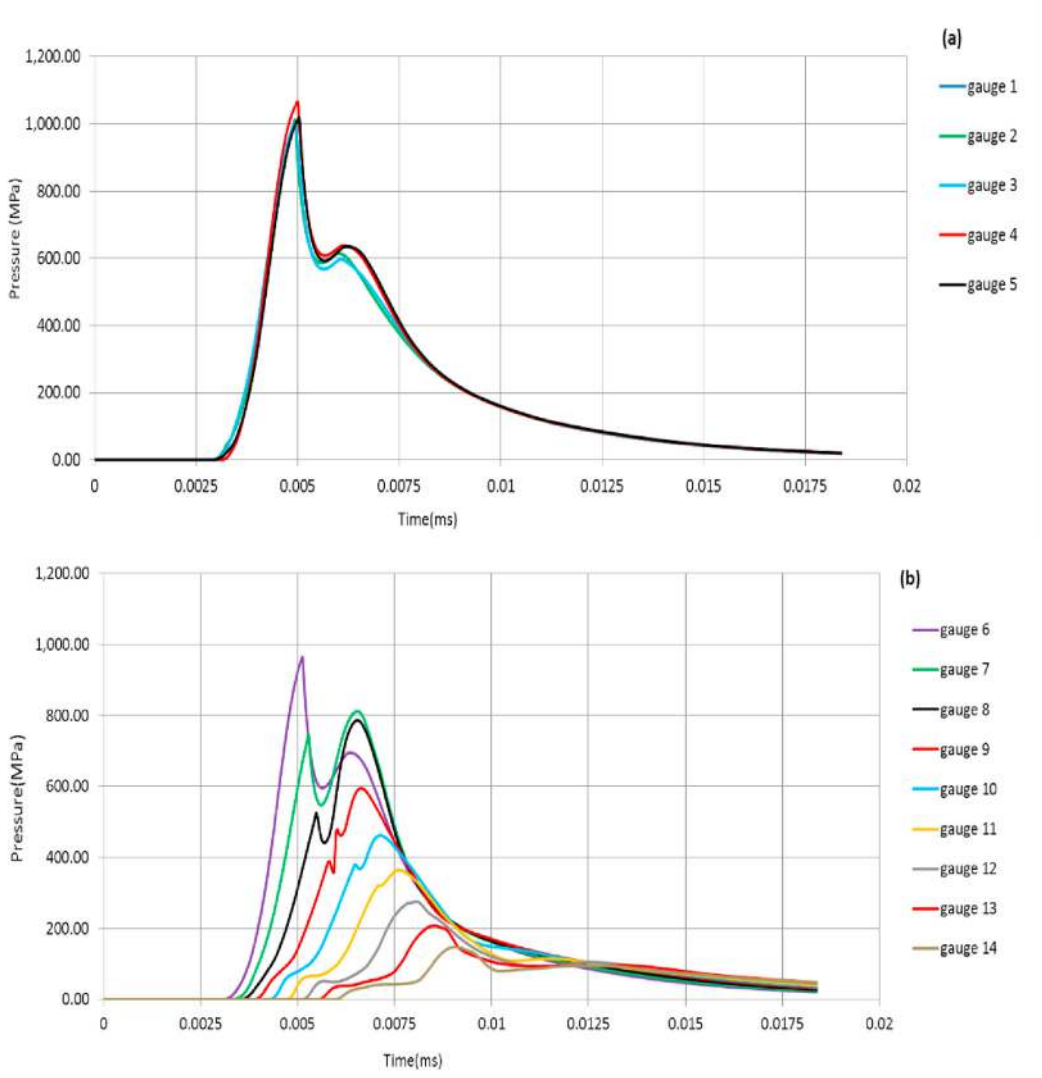

Fig. 7 – AUTODYN pressure history for different gauges (a) for center to 4 mm (b) for 6 mm–90 mm.

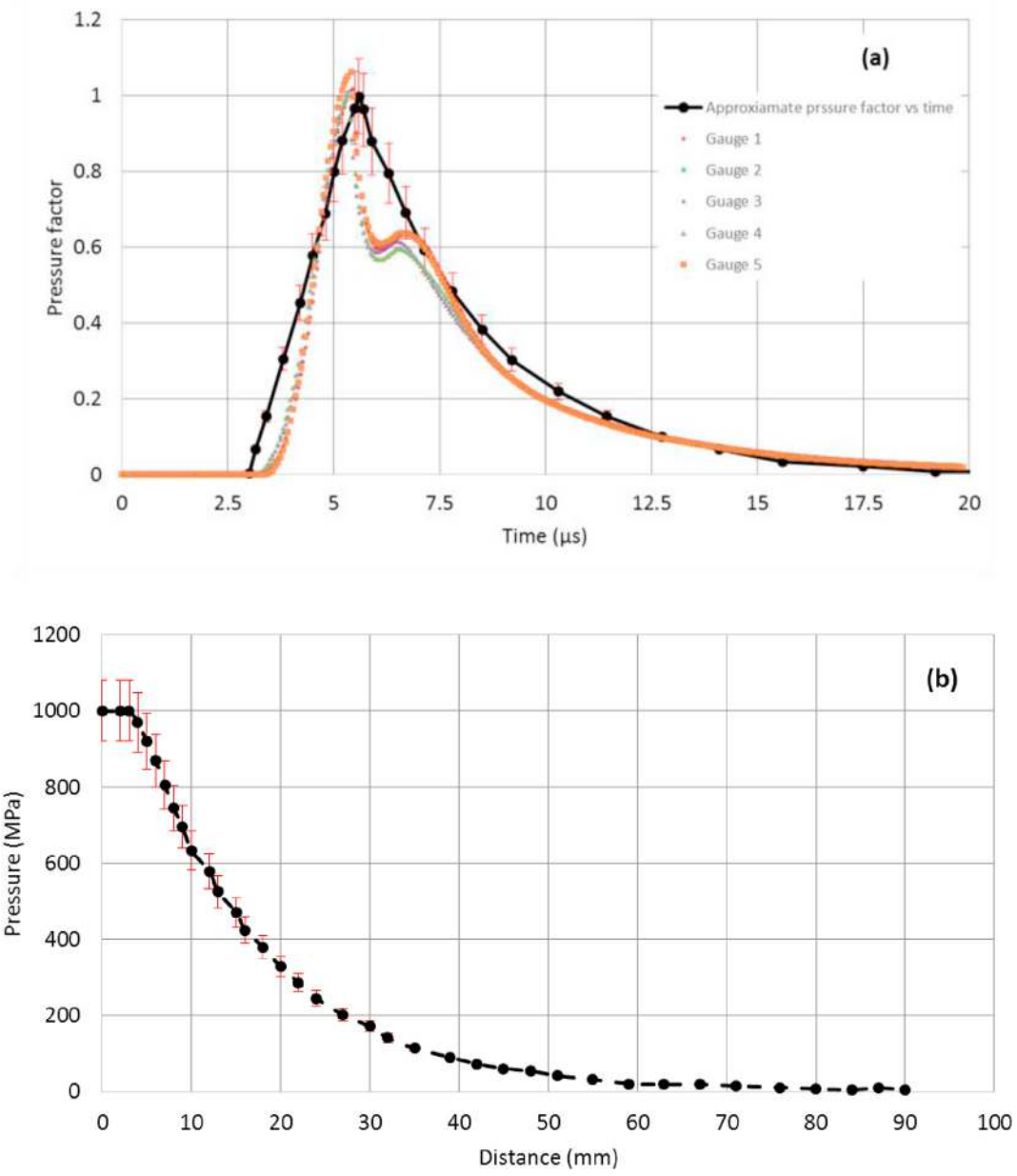

Fig. 8 – Pressure approximation pattern for 10 g emulsion in 4 mm SOD (a) time (b) radial distance.

difference in exponential decay functions, r_0, and r_b. From the approximation pattern of pressure time history at 50 mm SOD (Fig. 10) the pressure-time function is changed—as represented by Eq. (13).

$$p_{(t)} = \begin{cases} 0, & time \le t_{peak} \\ e^{-k_2\left(\frac{time - t_{peak}}{t_{death}}\right)}, & t_{peak} < time \le t_{death} \\ 0, & time > t_{death} \end{cases} \quad (13)$$

From AUTODYN, the pressure is constant for 30 mm from the center of the plate (r_0 = 30 mm) and r_b = 150 mm, which means the blast pressure uniformly covers the whole surface of the aluminum sheet at 50 mm SOD. The degradation factor in pressure distribution (K_1) is chosen at 0.027/mm, K_2 factor which effects time degradation on the pressure after the explosion is chosen at 4.2, t_{peak} = 20 μs and t_{death} = 75 μs. By comparing the two SODs, it is evident for the same mass of explosive the reflected peak pressure in 4 mm SOD is higher than 50 mm SOD but the duration time and exposed area is higher for 50 mm SOD. The total impulse loading can be found by the following equation [32]:

$$I = 2\pi \int_0^{\infty} \int_0^{r} rP(r,t)drdt \quad (14)$$

where I is total impulse, which can be found from the experiment, t is time and r is the distance from the centre of plate. When the explosive is located at very close range, the impulse pressure does not have enough time to convert to a uniform

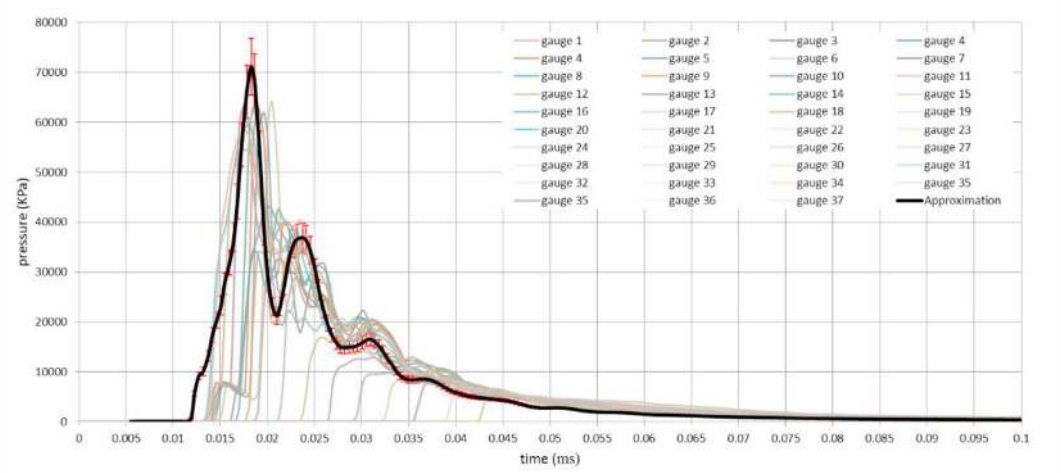

Fig. 9 – Pressure-time distribution for SOD 50 mm and 10 *g* emulsion.

distribution over the sheet blank. Therefore, applying different individual gauges in different locations to find the pressure-time history is essential. By substituting the pressure and time history functions for corresponding stand-off distances in Eq. (13), the values of maximum reflected pressure for different SODs can be found. The maximum reflected pressure for 10 *g* spherical emulsion at 4 mm and 50 mm SODs are 1160 MPa and 60 MPa, respectively.

3.2. *Finite element model*

To simulate the high-speed deformation process, a solid three-dimensional model was generated. To produce the non-uniform pressure history as a function of time and distribution, a FORTRAN-based computer code was implemented in ABAQUS from a user-defined subroutine VDLOAD [33]. Using Eqs. (11)–(14), the results were used to estimate the impulse energy for different SODs and charged mass. To reduce the computational time a one-quarter symmetry model was generated and analysed. Fig. (10) shows the 3D finite element model analysed in this study.

The model was built up with continuum 3D 8-noded elements with reduced integration ability (C3D8R). A mesh convergence study, regarding the stable plastic strain, was carried out and the minimum element size of 1.5 mm was selected for the exposed area. The Johnson–Cook material

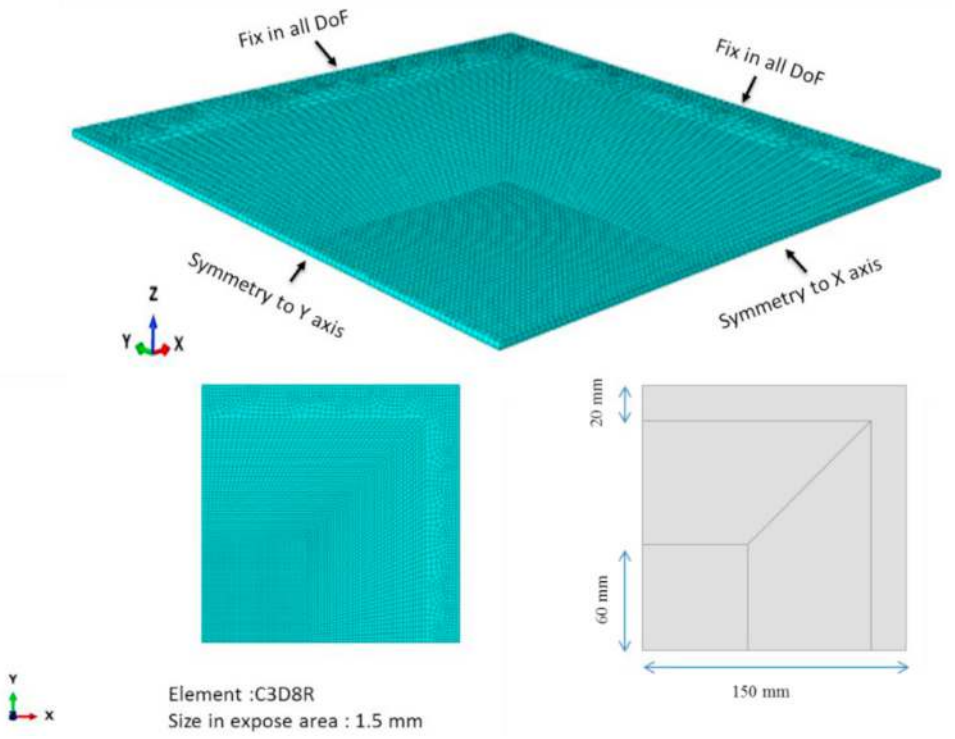

Fig. 10 – One quarter FE model for AL2024-T3 under impulsive loading.

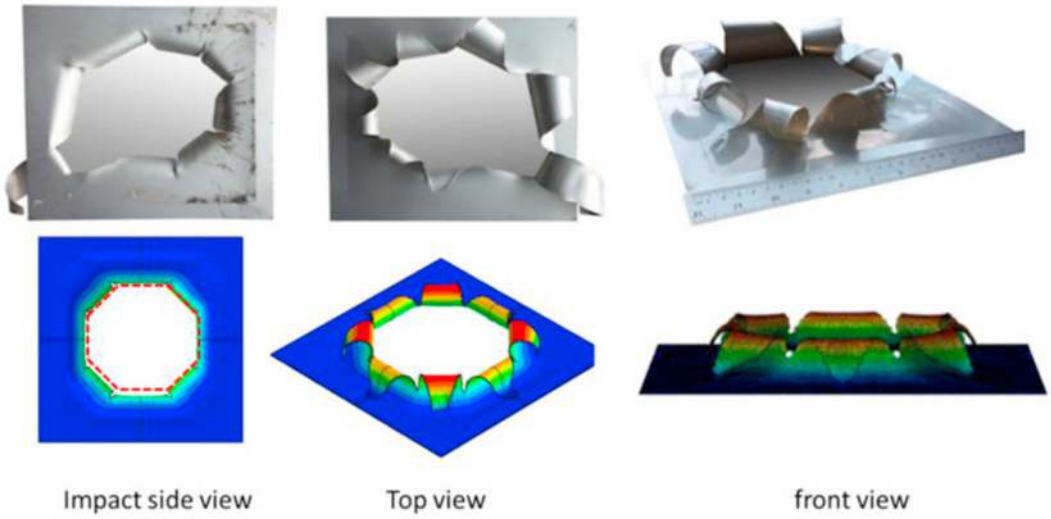

Fig. 11 – Comparison between FE modelling and experimental results of Al-10-4 exposed to impulse 6.6 N.s.

model in Table 1 was assigned to the FE model. The damage initiation and element deletion processes were adhered to according to Eq. (10). The energy balance analysis was performed to justify the numerical procedure [34–36]. The usual boundary conditions were applied at the planes of symmetry. The outer edges were fixed in all degrees of freedom and the inner edges were constrained along *x*- and *y*-axes respectively. The model was free to move in the z-direction.

4. Results

4.1. *Effect of close range impulse*

The shape deformed from 4 mm SOD impulse, from the test and FE simulation are compared in Fig. 11. The figure shows hexagon-shaped perforation with petalling in 8 tulips. The overall damage, in terms of deformation and perforation shape, shows good correlation between the experimental and the FE simulation results. It was observed that the release of impulsive energy in very close range to the specimens caused all the energy to fracture the sample. There is no sign of global lateral deformation of the sample. In a very short time interval after detonation (less than 5 μs) the crack initiation process began and propagated until the shock wave is nullified.

4.2. *Transient response in close-range impulse*

The transient response of sample Al-10-4 exposed to the close-field impulse of 6.6 N.s at 4 mm SOD is difficult to obtain experimentally. The difficulty of monitoring the transient responses of samples in blast tests is the main reason to consider a solution via FE modelling. The transient response is demonstrated as vertical displacement counterplots. At time step 4 μs after detonation the acting pressure triggers perforation. When the incrementation time is increased to 800 μs, the cracks around perforation hole grow and the outward tulips are clearly observed. The permanent deformation and damage of the aluminium sheet is shown in Fig. 12.

4.3. *Effect of mid-range impulse*

When the SOD is increased from 4 mm to 50 mm the impulsive energy from the charged mass of 10 *g* is reduced to 3.6 N.s. The reduced impulsive energy as well as the larger SOD helps the specimen from being damaged by permanent plastic deformation only. From previous research on the SOD value of either 4 mm or 50 mm are considered as near-field range explosions. However, changing the SOD from very close range to mid-range, the shock wave the structure behaves differently. Therefore, for a complete structural integrity assessment a further study is necessary on different ranges of shock waves. Fig. 13 compares the permanent deformed shape from experimental test and from FE modelling when the structure is placed at 50 mm SOD. The close correlation of maximum deflection from FE modelling and blast tests show that the applied shock wave from the blast test has been selected correctly and the FE model is validated.

5. Discussion

The results for the different test conditions are summarised in Table 2. Two main types of damage have been observed—global deformation with cap, and petalling. In the case of 4 mm SOD, the samples do not show any wrinkles around the boundary, but by changing the SOD to 50 mm many winkles appeared. Moreover, for 50 mm SOD, in-plane bulking appears and the presence of plastic hinge lines from the corner of the boundary to the centre of the aluminium sheet (along a 45-degree direction). No perforation is observed for this sample and the maximum back-face deflection reaches 34.8 mm. In

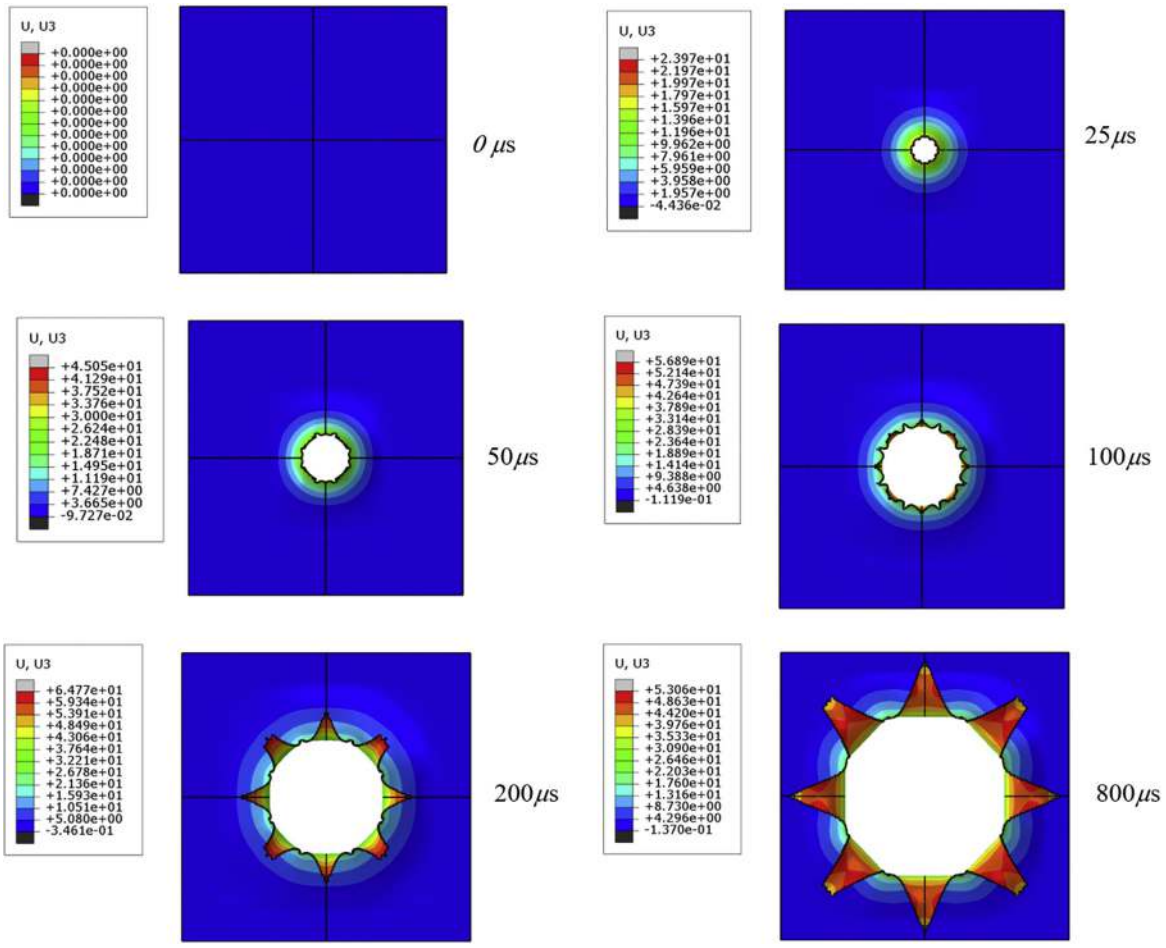

Fig. 12 – The transient response of aluminum sheet in impulse of 6.7 N.s on 4 mm SOD.

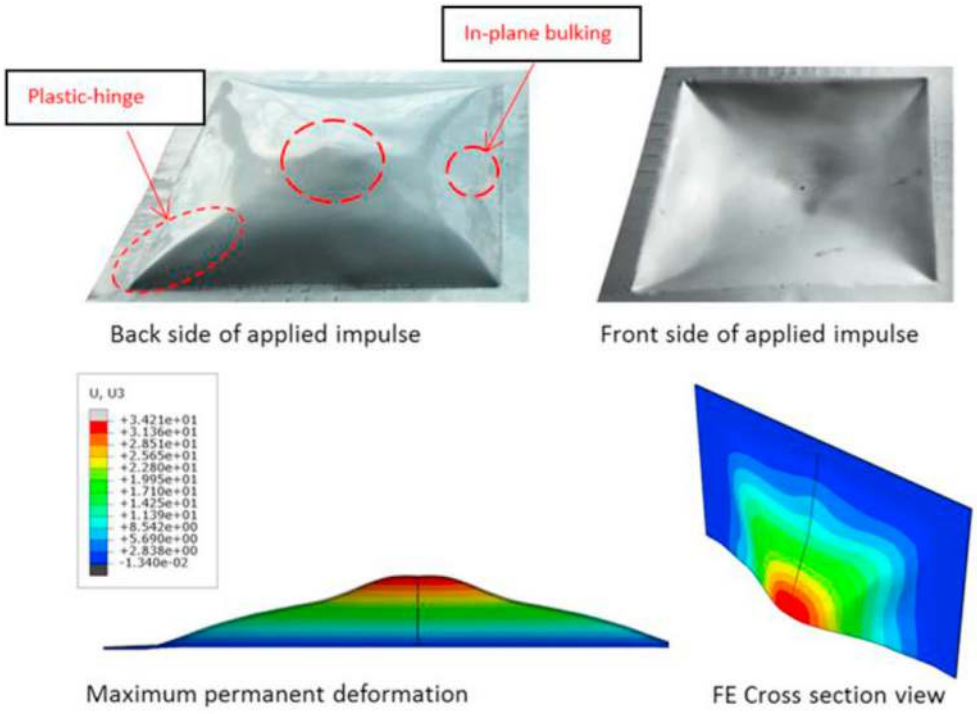

Fig. 13 – Comparison between FE and experimental results of Al-10-50 expose to impulse 3.6 N.s.

metal forming applications, the present study can be applied to calculate the optimum amount of explosive and SOD so as to avoid the presence of boundary wrinkles.

5.1. *Effect of different impulse energies*

The initial pressure (P_0) is one of the effective parameters in impulse calculation. Substitution of different values of P_0 in Eq. (11) leads to different values of impulse, and for the same SOD the maximum deflection and panel response can be different. Fig. 14 compares the different values of plastic deformation with different P_0 and impulse energies. The values of $P_0 = 60$ MPa and $I = 3.72$ N.s were the closest cases to the experimental test. The results from the experimental repetition (five replicates for each SOD) in Fig. 14 are presented with ±3% error that is shown with error bars.

By increasing the impulse to 6.6 N.s in 50 mm SOD, the maximum reflected peak pressure reaches 108 MPa. The aluminium sheet petals in 8 tulips. The results for the corresponding sample are shown in Fig. 15.

When the impulse for SODs at 4 mm and 50 mm is kept at a constant of 6.6 N.s, the peak reflected pressures for corresponding SODs are 1160 MPa and 108 MPa, respectively. Despite the peak reflected pressure for SOD 4 mm is around 10 times higher than SOD 50 mm, the damage in SOD 50 mm is much more severe (comparing the results from Figs. 11 and 15). The reason is that, the pressure degradation factor on the exposed area and the degradation time factor. At a SOD of 50 mm, the degradation time factor is 46%, and the pressure degradation factor is 60% less than corresponding factors at SOD 4 mm. The degradation from these two parameters cause more exposed area and more time-engagement with the impulsive loading and finally leads to more damage to the structure. Therefore, it cannot be directly interpreted that, by increasing the stand-off distance the structure can be protected against impulsive loading. As observed and explained, these two parameters have crucial roles and should be considered, especially in cladding structure design. For the explosive in the cylinder shape, the researchers investigated the blast pressure characterisation at a constant stand-off distance of 14 mm [10] and 50 mm [31]. By comparing the pressure degradation factor for cylinder explosives [31] and spherical explosives in this work, it is evident the pressure degradation factor for the cylinder explosive is 0.067 1/mm and for spherical explosive is 0.027 1/mm, which means in a mid-range explosion (SOD 50 mm) the pressure degradation for spherical explosive is less than the cylinder shap, and will engage an increased exposed area.

Table 2 – Stand-off distance, weight of explosive, the calculated impulse for the corresponding mass of explosive, maximum back face deflection and failure mode.

AL sheet code	Mass of charge (*g*)	SOD (mm)	Impulse (N.s)	Failure mode	deflection (mm)
Al-**10-4**	10	4	6.6	Tulip (petalling)	–
Al-**10-50**	10	50	3.6	Global deformation	34.8

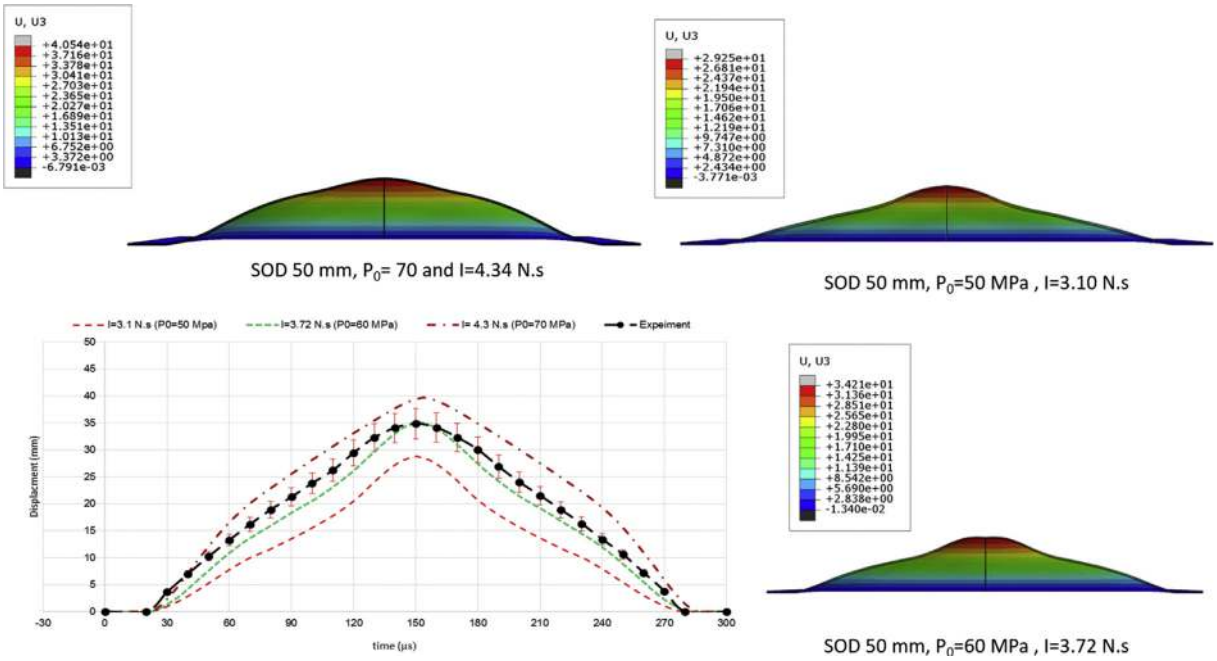

Fig. 14 – Comparison between FE modelling and experimental results of Al-10-50 expose to different impulse energies.

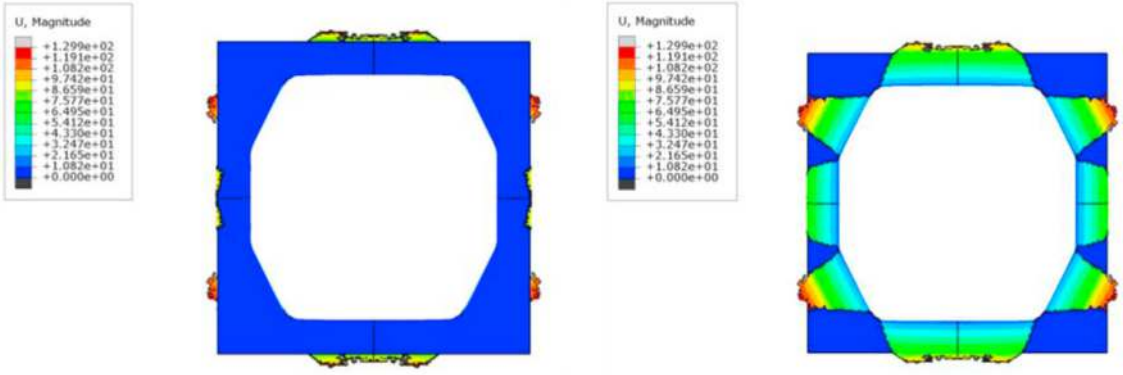

Fig. 15 – The results for SOD 50 mm when expose to impulse 6.6 N.s.

6. Conclusion

Aluminium 2024-T3 alloy sheets were used in a blast test with different stand-off distances and a constant charged mass, to investigate the effect of near-field shock waves. The transient behaviour was measured through permanent plastic deformation and perforation damage. A 4-cable instrumented pendulum blast set-up was prepared to carry out the test. The results of the blast test were used to simulate the pressure history from different SODs. A numerical finite element analysis was then carried out using commercial code in ABAQUS/Explicit. A user-defined subroutine was implemented in the ABAQUS solver to model non-uniform pressure field. The FE modelling prediction was then compared with the experimental results. The comparisons indicate that the material constitutive models and failure criteria were able to capture some high strain-rate failure features in the aluminium alloy sheets, such as petalling and perforation failure. By using the FE model more attention was focussed on the transient deformation process to analyse sheet behaviour. For stand-off distance, the effect of an increase from 4 mm to 50 mm becomes significant when the damage changes from a highly localised perforation to a global deformation. This implies that an instant failure model can be a useful tool to assess blast failures of metallic panel face-sheets in different kinds of composite stacking. In small stand-off distance the peak reflected pressure is a critical parameter, while by increasing the SOD, the duration time and exposed area are increased and these parameters are more critical than peak reflected pressure and need to be considered in structure design.

The findings are summarised as follow:

- In the experiment section:
  - o The effect of SOD on the aluminium sheet, subjected to the constant mass of a spherical shape emulsion explosive was studied from close-to mid-range explosions. The results indicate that by increasing the SOD, the damage form is dominated by global deformation rather than localised perforation.
  - o The effect of spherical explosive geometry on the blast pressure characterisation were highlighted by a comparison with available results.
- In the FE section:
  - o The blast pressure distribution and pressure-time functions for close- and mid-range explosions were found from AUTODYN and implemented into ABAQUS through a VDLOAD subroutine to validate the experimental results.
  - o The blast pressure characterisation such as peak reflected pressure, pressure-radial position degradation factor, and pressure-time degradation factor were highlighted for close-range and mid-range explosions. The results indicate that for the same mass of spherical explosive (10 g), the reflected peak pressure at 4 mm SOD is higher than 50 mm SOD, but the duration time and exposed area is higher for 50 mm SOD and causes the damage to shift from localised perforation to global deformation.
  - o The effect of blast pressure characterisations at mid-range explosion was discovered by promoting the impulses. The results indicate that by increasing the impulse, the in-plane buckling disappears and the damage of the target is dominated by increased global deformation the effect of SOD was studied by exposing the target to the same impulse load. The roles of pressure degradation and time-degradation factors in mid-range explosions are more crucial as the results indicate a higher SOD will cause the target to suffer more damage.

Data availability statement

The raw/processed data required to reproduce these findings cannot be shared at this time as the data also forms part of an ongoing study. The relevant data can be made available on request.

Declaration of Competing Interest

The authors declare that they have no known competing financial interests or personal relationships that could have appeared to influence the work reported in this paper.

Acknowledgements

This work was supported by Universiti Teknologi Malaysia collaborative research grant (Grant No. Q.J130000.2409.07G99) and fundamental grant scheme (Grant No. RJ 130000.7351.4B553). The authors wish to thank National Natural Science Foundation of China for their support (Grant No.11772215) as the technical and experimental assistance. The research was funded by the Ministry of Education, Youth, and Sports of the Czech Republic and the European Union (European Structural and Investment Funds Operational Program Research, Development, and Education) in the framework of the project "Modular platform for autonomous chassis of specialized electric vehicles for freight and equipment transportation", Reg. No. CZ.02.1.01/0.0/0.0/16_025/0007293, as well as the financial support from internal grants in the Institute for Nanomaterials, Advanced Technologies and Innovations (CXI), Technical University of Liberec (TUL). It was also supported by Universiti Putra Malaysia under Putra Grant No. GP/2018/9635100.

REFERENCES

[1] Li Y, Lv Z, Wang Y. Blast response of aluminum foam sandwich panel with double V-shaped face plate. Int J Impact Eng 2020 Jul 15:103666.
[2] Nia AB, Yahya MY, Ayob A, Nejad AF. Optimization of graded metallic foam subjected to impulsive loading through DOE approach. In: In 2018 9th international conference on mechanical and aerospace engineering (ICMAE). IEEE; 2018 Jul 10. p. 295–9.
[3] Pineau A, Benzerga AA, Pardoen T. Failure of metals I: brittle and ductile fracture. Acta Mater 2016 Apr 1;107:424–83.
[4] Sadighi M, Alderliesten RC, Benedictus R. Impact resistance of fiber-metal laminates: a review. Int J Impact Eng 2012 Nov 1;49:77–90.
[5] Jacob N, Nurick GN, Langdon GS. The effect of stand-off distance on the failure of fully clamped circular mild steel plates subjected to blast loads. Eng Struct 2007 Oct 1;29(10):2723–36.
[6] Langdon GS, Lemanski SL, Nurick GN, Simmons MS, Cantwell WJ, Schleyer GK. Behaviour of fibre–metal laminates subjected to localised blast loading: part I – experimental observations and failure analysis. Int J Impact Eng 2007;34:1202–22.
[7] Lemanski SL, Nurick GN, Langdon GS, Simmons MS, Cantwell WJ, Schleyer GK. Behaviour of fibre–metal laminates subjected to localised blast loading: part II – quantitative analysis. Int J Impact Eng 2007;34:1223–45.
[8] Langdon GS, Nuric GN, Lemanski SL, Simmons MS, Cantwell WJ, Schleyer GK. Failure characterisation of blast-loaded fibre–metal laminate panels based on aluminium and glass-fibre reinforced polypropylene. Compos Sci Technol 2007;67:1385–405.
[9] Mehreganian N, Louca LA, Langdon GS, Curry RJ, Abdul-Karim N. The response of mild steel and armour steel plates to localised air-blast loading-comparison of numerical modelling techniques. Int J Impact Eng 2018 May 1;115:81–93.
[10] Sitnikova E, Guan ZW, Schleyer GK, Cantwell WJ. Modelling of perforation failure in fibre metal laminates subjected to high impulsive blast loading. Int J Solid Struct 2014 Sep 1;51(18):3135–46.
[11] Bonorchis D, Nurick GN. The influence of boundary conditions on the loading of rectangular plates subjected to localised blast loading - importance in numerical simulations. Int J Impact Eng 2009;36:40–52.
[12] Bimha RE. Response of thin circular plates to central blast loading. Doctoral dissertation. University of Cape Town; 1996.

[13] Balden VH, Nurick GN. Numerical simulation of the post-failure motion of steel plates subjected to blast loading. Int J Impact Eng 2005 Dec 1;32(1–4):14–34.
[14] ANSYS/Autodyn-2D and 3D, Version 6.1. User Documentation.
[15] Syed ZI, Mohamed OA, Rahman SA. Non-linear finite element analysis of offshore stainless steel blast wall under high impulsive pressure loads. Procedia Eng 2016 Jan 1;145:1275–82.
[16] Mahmood Y, Dai K, Chen P, Zhou Q, Bhatti AA, Arab A. Experimental and numerical study on microstructure and mechanical properties of Ti-6Al-4V/Al-1060 Explosive Welding. Metals 2019 Nov;9(11):1189.
[17] Mouritz AP. Advances in understanding the response of fibre-based polymer composites to shock waves and explosive blasts. Compos Appl Sci Manuf 2019 Oct 1;125:105502.
[18] Cimpoeru SJ, Ritzel DV, Brett JM. Physics of explosive loading of structures. In: In explosion blast response of composites. Woodhead Publishing; 2017 Jan 1. p. 1–22.
[19] Dewey JM. Measurement of the physical properties of blast waves. In: In experimental methods of shock wave research. Cham: Springer; 2016. p. 53–86.
[20] Needham CE. Blast wave propagation. In blast waves. Cham: Springer; 2018. p. 97–120.
[21] Hunter KS, Geers TL. Pressure and velocity fields produced by an underwater explosion. J Acoust Soc Am 2004 Apr;115(4):1483–96.
[22] Kinney GF, Graham KJ. Explosive shocks in air. Springer Science & Business Media; 2013 Nov 11.
[23] Sanborn MJ. Experimental methods for understanding the behavior and residual capacity of bolts and steel bolted connections under impulsive loads. Doctoral dissertation. Georgia Institute of Technology; 2018.
[24] Tekalur SA, Bogdanovich AE, Shukla A. Shock loading response of sandwich panels with 3-D woven E-glass composite skins and stitched foam core. Compos Sci Technol 2009 May 1;69(6):736–53.
[25] Ngo T, Mendis P, Gupta A, Ramsay J. Blast loading and blast effects on structures–an overview. Electron J Struct Eng 2007 Jan;7(S1):76–91.
[26] Jing L, Wang Z, Zhao L. Measurement of impulse acted on a structure subjected to blast loading. J ExpMech 2009;24:151–6.
[27] Senthil K, Iqbal MA, Arindam B, Mittal R, Gupta NK. Ballistic resistance of 2024 aluminium plates against hemispherical, sphere and blunt nose projectiles. Thin-Walled Struct 2018 May 1;126:94–105.
[28] Peirovi S, Pourasghar M, Nejad AF, Hassan MA. A study on the different finite element approaches for laser cutting of aluminum alloy sheet. Int J Adv Manuf Technol 2017 Oct 1;93(1–4):1399–413.
[29] Castedo R, Natale M, López LM, Sanchidrián JA, Santos AP, Navarro J, et al. Estimation of Jones-Wilkins-Lee parameters of emulsion explosives using cylinder tests and their numerical validation. Int J Rock Mech Min Sci 2018 Dec 1;112:290–301.
[30] Karagiozova D, Langdon GS, Nurick GN, Yuen SC. Simulation of the response of fibre–metal laminates to localised blast loading. Int J Impact Eng 2010 Jun 1;37(6):766–82.
[31] Langdon GS, Karagiozova D, Von Klemperer CJ, Nurick GN, Ozinsky A, Pickering EG. The air-blast response of sandwich panels with composite face sheets and polymer foam cores: experiments and predictions. Int J Impact Eng 2013 Apr 1;54:64–82.
[32] Bassiri Nia A, Xin L, Yahya MY, Ayob A, Farokhi Nejad A, Rahimian Koloor SS, et al. Failure of glass fibre-reinforced polypropylene metal laminate subjected to close-range explosion. Polymers 2020;12:2139.
[33] Abaqus V. 6.14 documentation, vol. 651. Dassault Systemes Simulia Corporation; 2014. 6-2.
[34] Farokhi Nejad A, Alipour R, Shokri Rad M, Yazid Yahya M, Rahimian Koloor SS, Petrů M. Using finite element approach for crashworthiness assessment of a polymeric auxetic structure subjected to the axial loading. Polymers 2020;12:1312.
[35] Farokhi Nejad A, Chiandussi G, Solimine V, Serra A. Study of a synchronizer mechanism through multibody dynamic analysis. Proc Instit Mech Eng Part D: J Auto Eng 2019;233(6):1601–13.
[36] Nejad Farokhi A, Chiandussi G, Solimine V, Serra A. Estimation of the synchronization time of a transmission system through multi body dynamic analysis. Int J Mech Eng Robot Res 2017;6(3):232–6.